



Chinese Pharmaceutical Association
Institute of Materia Medica, Chinese Academy of Medical Sciences

Acta Pharmaceutica Sinica B

www.elsevier.com/locate/apsb
www.sciencedirect.com



ORIGINAL ARTICLE

Nanoparticles (NPs)-mediated Siglec15 silencing and macrophage repolarization for enhanced cancer immunotherapy



Xiaodi Liu^{a,b,†}, Qi Zhang^{b,c,†}, Yixia Liang^c, Shiyu Xiong^b, Yan Cai^d,
Jincheng Cao^b, Yanni Xu^b, Xiaolin Xu^b, Ye Wu^b, Qiang Lu^a,
Xiaoding Xu^{b,c,*}, Baoming Luo^{b,*}

^aDepartment of Ultrasound, Laboratory of Ultrasound Imaging and Drug, West China Hospital, Sichuan University, Chengdu 610041, China

^bDepartment of Ultrasound, Sun Yat-sen Memorial Hospital, Sun Yat-sen University, Guangzhou 510120, China

^cGuangdong Provincial Key Laboratory of Malignant Tumor Epigenetics and Gene Regulation, Sun Yat-sen Memorial Hospital, Sun Yat-sen University, Guangzhou 510120, China

^dDepartment of Ultrasound, Central People's Hospital of Zhanjiang, Zhanjiang 524045, China

Received 16 April 2023; received in revised form 7 July 2023; accepted 10 July 2023

KEY WORDS

Nanoparticles;
Tumor-associated
macrophages;
Macrophage
repoliarization;
T cell infiltration;
T cell proliferation;
Cancer immunotherapy;
Siglec15;
Hepatocellular carcinoma

Abstract T cell infiltration and proliferation in tumor tissues are the main factors that significantly affect the therapeutic outcomes of cancer immunotherapy. Emerging evidence has shown that interferon-gamma (IFN γ) could enhance CXCL9 secretion from macrophages to recruit T cells, but Siglec15 expressed on TAMs can attenuate T cell proliferation. Therefore, targeted regulation of macrophage function could be a promising strategy to enhance cancer immunotherapy *via* concurrently promoting the infiltration and proliferation of T cells in tumor tissues. We herein developed reduction-responsive nanoparticles (NPs) made with poly (disulfide amide) (PDSA) and lipid-poly (ethylene glycol) (lipid-PEG) for systemic delivery of Siglec15 siRNA (siSiglec15) and IFN γ for enhanced cancer immunotherapy. After intravenous administration, these cargo-loaded could highly accumulate in the tumor tissues and be efficiently internalized by tumor-associated macrophages (TAMs). With the highly concentrated glutathione (GSH) in the cytoplasm to destroy the nanostructure, the loaded IFN γ and si-Siglec15 could be rapidly released, which could respectively repolarize macrophage phenotype to enhance CXCL9 secretion for T cell infiltration and silence Siglec15 expression to promote T cell proliferation, leading to significant inhibition of hepatocellular carcinoma (HCC) growth when combining

*Corresponding authors.

E-mail addresses: luobm@mail.sysu.edu.cn (Baoming Luo), xuxiaod5@mail.sysu.edu.cn (Xiaoding Xu),

[†]These authors made equal contributions to this work.

Peer review under responsibility of Chinese Pharmaceutical Association and Institute of Materia Medica, Chinese Academy of Medical Sciences.

<https://doi.org/10.1016/j.apsb.2023.07.012>

2211-3835 © 2023 Chinese Pharmaceutical Association and Institute of Materia Medica, Chinese Academy of Medical Sciences. Production and hosting by Elsevier B.V. This is an open access article under the CC BY-NC-ND license (<http://creativecommons.org/licenses/by-nc-nd/4.0/>).

with the immune checkpoint inhibitor. The strategy developed herein could be used as an effective tool to enhance cancer immunotherapy.

© 2023 Chinese Pharmaceutical Association and Institute of Materia Medica, Chinese Academy of Medical Sciences. Production and hosting by Elsevier B.V. This is an open access article under the CC BY-NC-ND license (<http://creativecommons.org/licenses/by-nc-nd/4.0/>).

1. Introduction

The tumor immune microenvironment plays a pivotal role in regulating the prognosis of cancer patients^{1,2}. Immunotherapy, which is mostly carried out by cytotoxic CD8⁺ T cells, has shown promising potential for treatment³. Nevertheless, it is not completely understood which factors influence the likelihood of patient response to immunotherapy. At present, several factors have been recognized as predictors of immunotherapy response, including the mutational load of the tumor, the expression of target ligands such as PD-L1, and the infiltration of immunoreactive T cells⁴. Among them, the infiltration of cytotoxic CD8⁺ T cells has been widely used in clinics to predict the immunotherapy effect of various types of cancers (*e.g.*, breast, liver, colon, and lung cancer)⁵. Therefore, understanding the inherent mechanisms regulating the infiltration of cytotoxic CD8⁺ T cells into the tumor tissues is essential for the development of effective strategies to enhance cancer immunotherapy and improve the prognosis of cancer patients.

It is known that some chemokines (*e.g.*, CCL5, CXCL9, and CXCL10) are the main drivers for T cell engraftment in tumor tissues⁶. CCL5 and CXCL9 co-expression suggests immunoreactive tumors and response to PD-1/PD-L1 and CTLA4 blockade⁶. The CXCL10 also has been shown to be predictive of adoptive cellular therapy^{7,8}. It has been reported that interferon-gamma (IFN γ) is essential for the secretion of CXCL9 and CXCL10⁴. T cell activation and proliferation are other factors that influence the prognosis of cancer patients. Nevertheless, high serum concentration of IFN γ is associated with significant side effects and toxicities, such as fatigue, nausea, vomiting, neurotoxicity, and leukopenia⁹.

Recently, several studies have emphasized the role of macrophages expressing sialic acid-binding immunoglobulin-like lectin 15 (Siglec15) in repressing immune responses in the tumor microenvironment (TME). In cancer patients, Siglec15 is one of the newly discovered potential targets for next-generation immunotherapy¹⁰. Studies have reported that Siglec15 attends T cells proliferation by binding to receptors on T cells^{11,12}, another study has shown that Siglec15⁺ TAM presented an M2-like phenotype through interacting with tumor-expressed sialic acid¹³. Although immunotherapy holds great promise for combating cancer, its broader application is hindered by limited efficacy caused by an immunosuppressive tumor microenvironment and systemic toxicity. It has been reported that nanoparticle-targeted delivery systems could enhance immunotherapy on cancers^{14,15}. Studies have demonstrated that small interfering RNAs (siRNAs) can silence targeted gene expression¹⁶. However, due to its negatively charged nature, systemic administration of siRNA is challenging. Nanoparticles (NPs) have been regarded as an effective method for systemic siRNA delivery^{17–19}. More importantly, tumor microenvironments differ from those of normal tissue (*e.g.*, hypoxic, weakly acidic)²⁰, systemically delivering siRNA using stimuli-

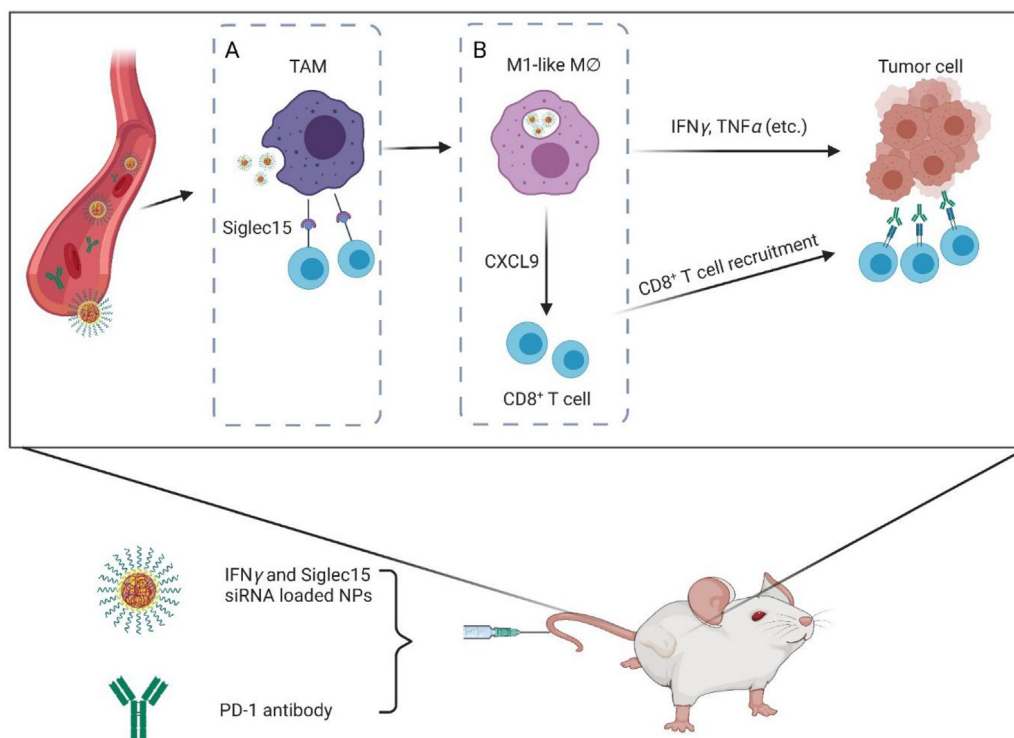
responsive NPs could not only prolong the blood circulation and tumor accumulation of siRNA, but also increase its cellular uptake and intracellular retention^{21–23}.

In this work, we found that both Siglec15 and CXCL9 are mainly localized in tumor associated macrophages (TAMs). Therefore, targeted regulation of TAMs function to concurrently increase the secretion of T cell infiltration-associated chemokines and suppress Siglec15 expression could be expected to enhance the efficacy of cancer immunotherapy. Along this principle and inspired by the advantages of delivering siRNA *via* stimuli-responsive nanoparticles, we herein developed a reduction-responsive nanoplatform, which is composed of a poly (disulfide amide) (PDSA) core and a lipid-poly (ethylene glycol) (lipid-PEG) shell to delivery IFN γ and Siglec15 siRNA (siSiglec15) and enhance liver cancer immunotherapy. The NPs would be efficiently internalized by tumor-associated macrophages and accumulate in the tumor tissues after being intravenously administrated. The highly concentrated glutathione (GSH) could cause NPs to dissociate in the cytoplasm, so the loaded IFN γ and siSiglec15 could be rapidly released to respectively repolarize TAMs into M1-like macrophages and silence Siglec15 expression. With this phenotype transition and Siglec15 silencing, the infiltration of cytotoxic CD8⁺ T cells in tumor tissues is dramatically enhanced and their proliferation is also promoted, thereby achieving significant inhibition of tumor growth on subcutaneous and orthotopic hepatocellular carcinoma (HCC) tumor models when combining with the immune checkpoint inhibitor (*i.e.*, PD1 antibody) (Scheme 1).

2. Materials and methods

2.1. Materials

We purchased dimethyl sulfoxide (DMSO), Dimethylformamide (DMF), and reductive glutathione (GSH) from Sigma–Aldrich and used them as received. 1,2-distearoyl-*sn*-glycero-3-phosphoethanolamine-*N*-[methoxy (polyethylene glycol)-3000] (DSPE-PEG3k) was purchased from Avanti (Avanti Polar Lipids, AL, USA). Based on our previous studies, poly (disulfide amide) (PDSA) and poly (disulfide amide) dendrimer (G0-C14) were synthesized²⁴. In this study, recombinant mCSF (mouse macrophage colony-stimulating factor) was purchased from Novus Biologicals (Novus Biologicals, Littleton, USA). Siglec15 siRNA (sense: 5'-GCUCCAGAUGGGAUCCCUUTT-3', antisense: 5'-AAGGGAUCCCAUCUGGAGCTT-3') was purchased from IGE BIOTECHNOL (IGE BIOTECHNOL, Guangzhou, China). The Cy5-labeled siRNA was purchased from Hongxun Biotechnologies (Hongxun Biotechnologies, Guangzhou, China). We purchased Dulbecco's modified Eagle medium (DMEM), penicillin-streptomycin, fetal bovine serum (FBS), and trypsin from Biological Industries (Biological Industries, IL, Israel) and used them as received.



Scheme 1 Schematic illustration of the therapeutic effects of reduction-responsive NPs (IFN γ /siSiglec15) on recruitment and activation of CD8 $^{+}$ T cells. IFN γ and siSiglec15 were co-encapsulated into reduction-responsive NPs, and then intravenously injected into HCC tumor bearing mice. The IFN γ and siSiglec15 loaded NPs could accumulate in tumor tissues and released (A) siSiglec15 to silence the expression of Siglec15, leading to the reverse of the T cell suppression induced by Siglec15; (B) IFN γ to repolarize TAMs to M1 phenotype, leading to the secretion of CXCL9. This reduction-responsive nanoplatform could effectively recruit and activate CD8 $^{+}$ T cells to enhance the efficacy of anti-PD1 antibodies and inhibit tumor growth. This figure was created using BioRender (<https://biorender.com>).

2.2. Patients and tissue samples

Tumor samples from the HCC patients were collected from Sun Yat-sen Memorial Hospital of Sun Yat-sen University. Informed consent was not required for a retrospective, case–control study. This study was approved by Sun Yat-sen Memorial Hospital’s Institutional Review Board (IRB) (SYSKY-2022-166-01). From March 2015 to June 2019, 64 patients with HCC underwent surgical resection at Sun Yat-sen Memorial Hospital with available samples were consecutively included in our current retrospective study. Other clinical data, such as age, sex, virus infection status, alcohol intake tumor size, and so on, were collected from the medical records. We obtained information on survival by reviewing medical records and conducting telephone interviews. Overall survival (OS) is defined as the number of days between surgery and death, or the last follow-up after surgery.

2.3. Online dataset

The correlation of Siglec15 expression in tumor and normal tissues of HCC patients from the TCGA database was acquired from Gene Expression Profiling Interactive Analysis (GEPIA) (<http://gepia.cancer-pku.cn/>). Single-cell RNA-Seq data are available from the liver cancer single-cell data under accession number GSE125449²⁵. The data were analyzed with an online database for single-cell transcriptome of tumor immune microenvironment (The scTIME Portal, <http://sctime.sklehabc.com/>).

2.4. Preparation and characterizations of siRNA/IFN γ -loaded NPs

The siRNA/IFN γ -loaded NPs were synthesized *via* the modified nanoprecipitation method in accordance with our previous reports²⁶. Briefly, 200 μ L of PDSA solution (20 mg/mL in DMF) was combined with 50 μ L of cationic lipid-like compound G0-C14 solution (5 mg/mL in DMF), 140 μ L of DSPE-PEG3k solution (20 mg/mL in DMF), 1 nmol of siRNA (0.1 nmol/ μ L in deionized water), and 10 μ g of IFN γ (1 mg/mL in deionized water). With continuous stirring (1000 rpm), the mixture was added dropwise to RNase-free water (5 mL). In order to remove organic solvents and free compounds from the formed NP suspension, an ultrafiltration device (EMD Millipore, Billerica, MA, USA, MWCO 100,000 kDa) and centrifugation were applied.

After washing with deionized water thrice (3 \times 5 mL), the final NPs [denoted NPs (IFN γ /siSiglec15)] were suspended in phosphate buffered saline (PBS) solution at an mRNA concentration of 0.1 nmol/ μ L and INF γ concentration of 10 μ g/mL. A dynamic light scattering method (Malvern Instruments, Pennsylvania, PA, USA) was used to determine the size and zeta potential of the nanoplatform. The NP morphology was visualized under a transmission electron microscope (TEM) (FEI, Hillsboro, OR, USA). To determine the encapsulation efficiency (EE) of siRNA and IFN γ , Cy5-labeled siRNA and Cy3-labeled IFN γ were encapsulated into the NPs according to the nanoprecipitation method described above. The fluorescence intensity of Cy5 and

Cy3 was measured on a TECAN Spark10 M microplate reader (Tecan Group Ltd., Männedorf, Switzerland), and EE of siRNA and IFN γ was calculated by comparing the fluorescence intensity of Cy5 and Cy3 to standard curves.

2.5. Cell culture

Hepa1-6 cells were cultured in DMEM medium supplemented with 10% FBS at 37 °C in a humidified atmosphere containing 5% CO₂.

2.6. Macrophages generation and differentiation

Mouse bone marrow-derived monocytes (BMDMs) were cultured in DMEM medium supplemented with 10% FBS and 20 ng/mL of mCSF at 37 °C in a humidified atmosphere containing 5% CO₂ for 7 days to differentiate into mature M0 macrophages. Briefly, bone marrow cells were collected from the femurs and tibias of C57BL/6 mice, then filtering through a 70 μ m membrane, red cell lysis buffer was applied to remove erythrocytes, and then the monocytes suspension was centrifuged at 350 *g* and collected. The obtained BMDM was suspended in DMEM medium containing 10% FBS, 20 ng/mL mCSF and 1% penicillin/streptomycin, and then transfer to 6-well plates.

To obtain TAMs, M0 macrophages were incubated at 37 °C in the presence of Hepa1-6 tumor cell culture supernatant^{27,28}. After a further 24 h incubation, Hepa1-6 tumor cell culture supernatant-induced tumor-associated macrophages were identified by analyzing the expression of CD206 and Arg-1 with real-time polymerase chain reaction (RT-qPCR) in a LightCycler 480 System (Roche, Rotkreuz, Switzerland) (Supporting Information Fig. S1).

2.7. In vitro gene silencing

TAMs were induced in 6-well plates (1 \times 10⁵ cells per well). After changing the medium, NPs (IFN γ /siSiglec15) were added. After 24 h of incubation, cells were washed with PBS buffer and incubated for an additional 48 h in a fresh medium. After discarding the medium, the cells were washed with PBS buffer, and the total protein was extracted with RIPA lysate supplemented with protease inhibitors. The protein levels of Siglec15 were examined by western blotting and immunofluorescence. The total RNA was extracted using an RNA extraction kit, and the mRNA level of Siglec15 was examined using RT-qPCR.

2.8. Detection of identification of macrophage phenotype and T cell infiltration level

A total of 1 \times 10⁵ TAMs were seeded per well in a 6-well plate and incubated in two mL of medium for 24 h. After treating the cells with the NPs (IFN γ /siSiglec15) at a siRNA dose of 25 nmol/L, the total RNA was extracted using an RNA extraction kit, and the mRNA level of M1 macrophages (CD86, IL-6, and iNOS) and M2 macrophages (Arg-1, IL-10, and CD206) was analyzed by RT-qPCR. The phenotypic polarization was observed by the fluorescence intensity of immunofluorescence CD206 staining (red fluorescence) and then viewed under a ZEISS 800 confocal laser scanning microscope. In addition, surface staining

of M1 (MHC-II) and M2 (CD206) was analyzed by flow cytometry (CytoFLEX, Beckman Coulter, Brea, CA, USA).

2.9. Chemotaxis assay and ELISA

We used a 24-well Boyden Chamber device with an 8.0 μ m pore size (Corning, NY, USA) to conduct the chemotaxis assay. A total of 1 \times 10⁵ TAMs were seeded into the lower chamber and the T cells derived from the mice's spleen were seeded into the upper chamber. The number of T cells was measured by flow cytometry stained with CD8 antibody.

2.10. Animals

We purchased C57BL/6 male mice (3–4 weeks old) from Guangdong Medical Lab Animal Center (Guangzhou, China). All *in vivo* studies were ethically approved by Institutional Animal Care and Use Committee at Sun Yat-sen University (SYSU-IACUC-2020-B033).

2.11. Establishment of subcutaneous and orthotopic tumors

Hepa1-6 cells were suspended in a mixture of PBS and Matrigel (1/1, *v/v*) at a concentration of 5 \times 10⁷ cells/mL, subcutaneous injection of 0.1 mL of cell suspension was performed in the mice's flanks and the tumor growth was monitored every two days. The tumor size was calculated with the following eq. (1):

$$V = W^2 \times L/2 \quad (1)$$

where *W* and *L* are the width and length of tumors, respectively.

When tumor xenografts had grown, tumors were harvested and cut into 1 mm pieces, which were implanted into the left lobes of the liver of other tumor-free mice. After 7 days, the resulting tumor volume was assessed using a small animal ultrasound system (Visual Sonics Vevo® 2100 system, Visual Sonics Inc. Toronto, ON, Canada). Hepa1-6 orthotopic tumor volumes were measured using a three-dimensional (3D) motor arm and MS400 transducer on a high-resolution ultrasound (Vevo®2100 system; Visual Sonics Inc. Toronto, ON, Canada). The orthotopic tumor sizes were monitored and reconstructed into 3D images for further analysis with the Visual Sonics Vevo®2100 system. The tumor-bearing mice were then randomly assigned to either control or different treatment groups, and tumor growth was observed every 4 days.

2.12. Macrophages repolarization and T cells recruitment in vivo

Hepa1-6 xenograft tumor-bearing mice were randomly divided into four groups (*n* = 3) and received intravenous injections of either (i) control NPs, (ii) NPs (IFN γ /siNC), (iii) NPs (siSiglec15), (iv) NPs (IFN γ /siSiglec15) for three consecutive days (0.5 nmol siRNA and 5 μ g IFN γ dose per mouse). The mice were sacrificed 24 h after the final injection and tumors were harvested for immunohistochemistry (IHC) and Western blot analysis of Siglec15 expression in the tumor tissues. In addition, the proportion of M1 and M2 macrophages through examining the MHC-II⁺/F480⁺ and CD206⁺/F480⁺ cells and the proportion of CD4⁺ and CD8⁺T cells in the tumors were obtained by flow cytometry.

The expression of CD206 in tumor sections was also used to identify the macrophage phenotype in tumor tissues.

2.13. Inhibition of subcutaneous tumor growth

Hepa1-6 subcutaneous tumor-bearing mice were randomly divided into seven groups ($n = 6$) and received intravenous injections of either (i) PBS, (ii) Control NPs, (iii) NPs (IFN γ /siNC), (iv) NPs (siSiglec15), (v) NPs (IFN γ /siSiglec15), (vi) anti-PD1 or (vii) anti-PD1 + NPs (IFN γ /siSiglec15). Tumor-bearing mice were injected with 0.5 nmol siRNA-loaded NPs every two days. Based on the method described above, the tumor growth was monitored every 2 days. Upon reaching 1000 mm³, the experiment is terminated. At the end of the experiment, all the tumors were collected according to the manufacturer's instructions.

2.14. Inhibition of orthotopic tumor growth

Hepa1-6 orthotopic tumor-bearing mice were randomly divided into six groups ($n = 5$) and received intravenous injections of either (i) Control NPs, (ii) NPs (IFN γ /siNC), (iii) NPs (siSiglec15), (iv) NPs (IFN γ /siSiglec15), (v) anti-PD1 or (vi) anti-PD1 + NPs (IFN γ /siSiglec15). Tumor-bearing mice were injected with 0.5 nmol siRNA and 0.5 μ g IFN γ -loaded NPs every two days. The mice were injected four times consecutively and the tumor growth was monitored every four days by ultrasonic scanning with a small ultrasound machine. The tumor volume was calculated by three-dimension reconstruction. Experiments with tumor-bearing mice were terminated when severe hepatic ascites are observed. At the end of the experiment, all the tumors were collected according to the manufacturer's instructions.

2.15. Statistical analysis

The data were presented as mean \pm SEM. Student's *t*-test, Log-rank (Mantel–Cox) test, and one/two-way ANOVA were performed for the statistical analysis. For tumor growth statistics, the non-parametric Mann–Whitney U rank sum test was performed to compare tumor volumes. A *P* value < 0.05 is considered statistically significant.

3. Results and discussion

3.1. Siglec15 expression is up-regulated in TAMs and predicts poor prognosis in HCC patients

It has been reported that Siglec15 is an immune suppressor with broad upregulation across several cancer types, which is one of the potential targets for cancer immunotherapy^{29,30}. Siglec15 is predominantly expressed on macrophages at a low level in physiological conditions, but can be upregulated by cytokines produced by tumor cells¹². We herein studied the expression of Siglec15 in HCC patients, we first investigated whether Siglec15 expression correlated with human HCC tissues. We observed a significant correlation between Siglec15 and HCC of The Cancer Genome Atlas (TCGA) (Fig. 1A). Siglec15 was significantly overexpressed in HCC tumor tissues ($n = 369$) compared to normal liver tissues ($n = 160$). To mimic tumor-associated macrophages (TAMs) formation, bone marrow derived macrophages (BMDMs) were cultured in the conditioned supernatant of Hepa1-6 cells according

to the previous studies^{27,28}. Compared to untreated BMDMs, we observed a higher mRNA and protein expression of Siglec15 in TAMs (Fig. 1B and C). Moreover, a set of surgically resected tumor samples were collected from HCC patients ($n = 64$) and performed immunohistochemistry (IF), we observed positive Siglec15 in 51.6% (33/64) of the patients. We further performed immunofluorescence (IF) to detect the relationship between Siglec15 and macrophages. In Fig. 1D and E, we could see that Siglec15 (red fluorescence) was primarily present on TAMs that were marked with green fluorescence using the CD68 antibody. However, it was also found in a few tumor cells and vascular endothelial cells. We did not detect Siglec15 on T cells or fibroblasts. These findings were aligned with previous research (Supporting Information Fig. S2)¹³.

In total, 64 patients were included in this study, the baseline patient clinicopathological characteristics were listed in Supporting Information Table S1, and the median age was 55 years (range: 25–78 years). At the end of the follow-up, 53.12% (34/64) of patients died from HCC (Fig. 1F and G). The median OS time was 37 months (ranging from two to 87 months). Kaplan–Meier curves showed that Siglec15 positivity was significantly associated with poorer OS ($P = 0.0364$) (Fig. 1F and G).

3.2. IFN γ is correlated with CXCL9 and T cell infiltration

In light of the important role that CD8⁺ T cells play in immune-mediated tumor inhibition and in predicting clinical prognosis, we selected CD8A as a gene marker for quantifying T cells in cancer. The expression of CD8A correlated consistently with that of CXCL9 and CXCL10 in HCC (Supporting Information Fig. S3A). Using single-cell sequencing data that was previously generated from HCC patients revealed that CXCL9 was predominantly expressed by macrophages and DCs (Fig. S3B)²⁵. Studies had demonstrated CXCL9 expressed by macrophages was important for the infiltration of T cells into tumors, which was induced by IFN γ ⁴. We also found that IFN γ expression was correlated with CXCL9 and CXCL10 (Fig. S3C). Compared to untreated TAMs, among all chemokines, only the mRNA expression of CCL5, CXCL9, and CXCL10 were significantly up-regulated after treatment with IFN γ (Fig. S3D).

3.3. NPs-mediated macrophage repolarization

We have demonstrated that Siglec15 was highly expressed on TAMs in HCC, and CXCL9, which contributed to T cell infiltration, was abundantly expressed in IFN γ treated TAMs. Then we constructed redox-responsive polymer hybrid NPs to silence Siglec15 expression and promote the secretion of CXCL9. The redox-responsive NPs were used to encapsulate IFN γ and siSiglec15 in this study. There were three components of this NP platform: amphiphilic cationic lipid G0-C14, reduction-responsive PDSA polymer, and DSPE-PEG3k. Aqueous siRNA and protein solutions are mixed with G0-C14, then mixed with PDSA polymer and DSPE-PEG_{3k}, followed by rapid stirring in DI water, with an average size of 116 nm with a narrow polydispersity index (<0.25), spherical NPs (IFN γ /siSiglec15) could be formed (Fig. 2A and B, Supporting Information Fig. S4). The zeta potentials of the control NPs, NPs (siSiglec15), and NPs (IFN γ /siSiglec15) were -0.71 , -3.98 , and -1.4 mV, respectively. Using Cy5 labeled-siRNA, the

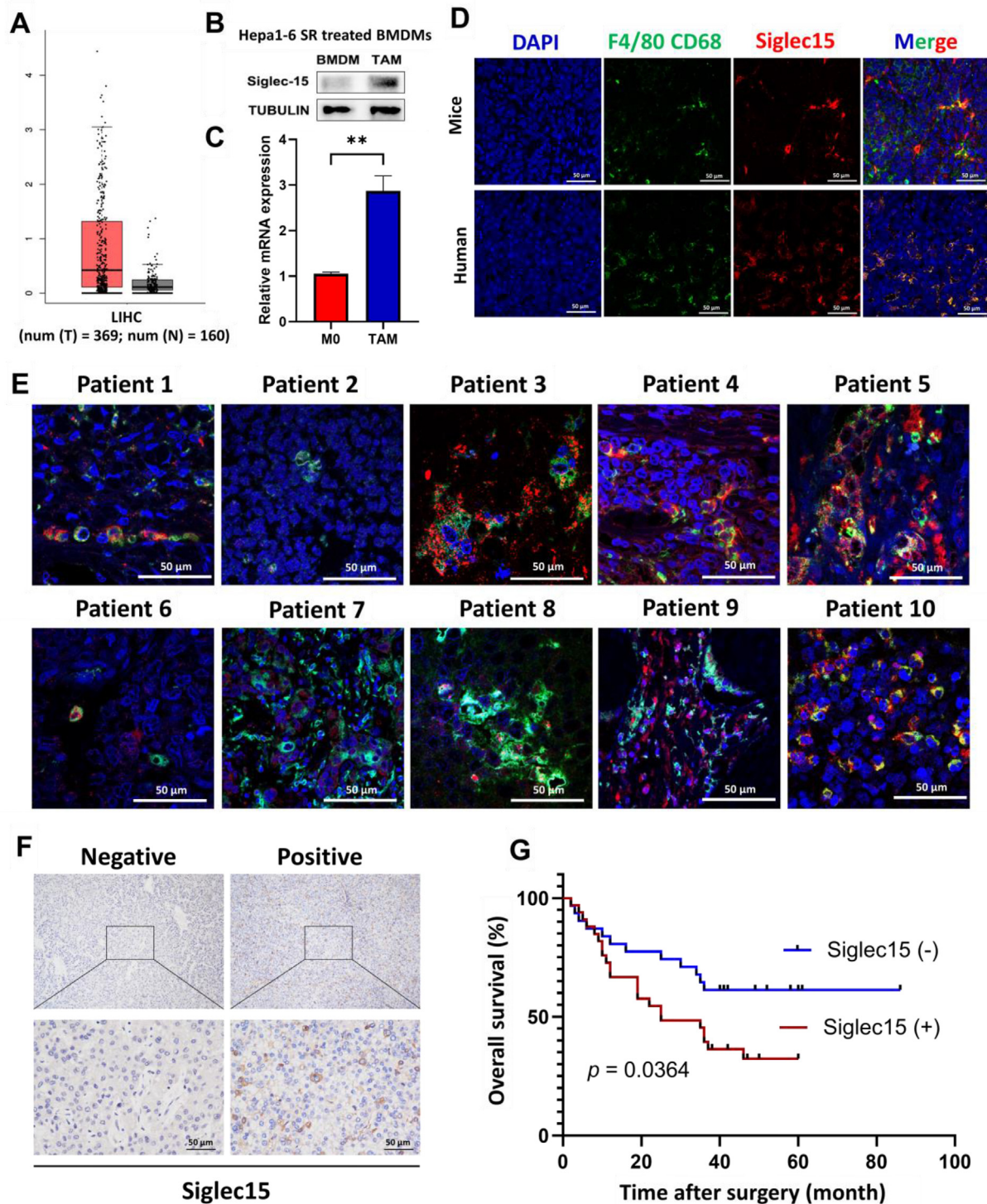


Figure 1 Expression of Siglec15 in HCC patients. (A) TCGA (The Cancer Genome Atlas) database showing Siglec15 expression in the adjacent ($n = 160$) and tumor tissues ($n = 369$) of hepatocellular carcinoma (HCC) patients. (B) Western blot analysis of Siglec15 expression in BMDMs generated from mice bones and tumor cells supernatant induced tumor-associated macrophages (TAMs). (C) qPCR analysis of Siglec15 expression in bone marrow derived macrophages (BMDMs) generated from mice bones and tumor cells supernatant induced TAMs. Data were presented as mean \pm SEM ($n = 3$). $***P < 0.005$ vs. indicated. (D, E) Immunofluorescence (IF) analysis of CD68 and Siglec15 co-expression in the tumor tissues of mice model and HCC patients. Scale bar = 50 μ m. (F) Immunohistochemistry (IHC) analysis of Siglec15 expression in HCC tissue samples. Scale bar, 50 μ m. (G) Kaplan–Meier survival curves for overall survival (OS) of patients with HCC according to Siglec15 expression. ($n = 33$ for Siglec15⁺ group and $n = 31$ for Siglec15⁻ group, $*P < 0.05$ vs. indicated).

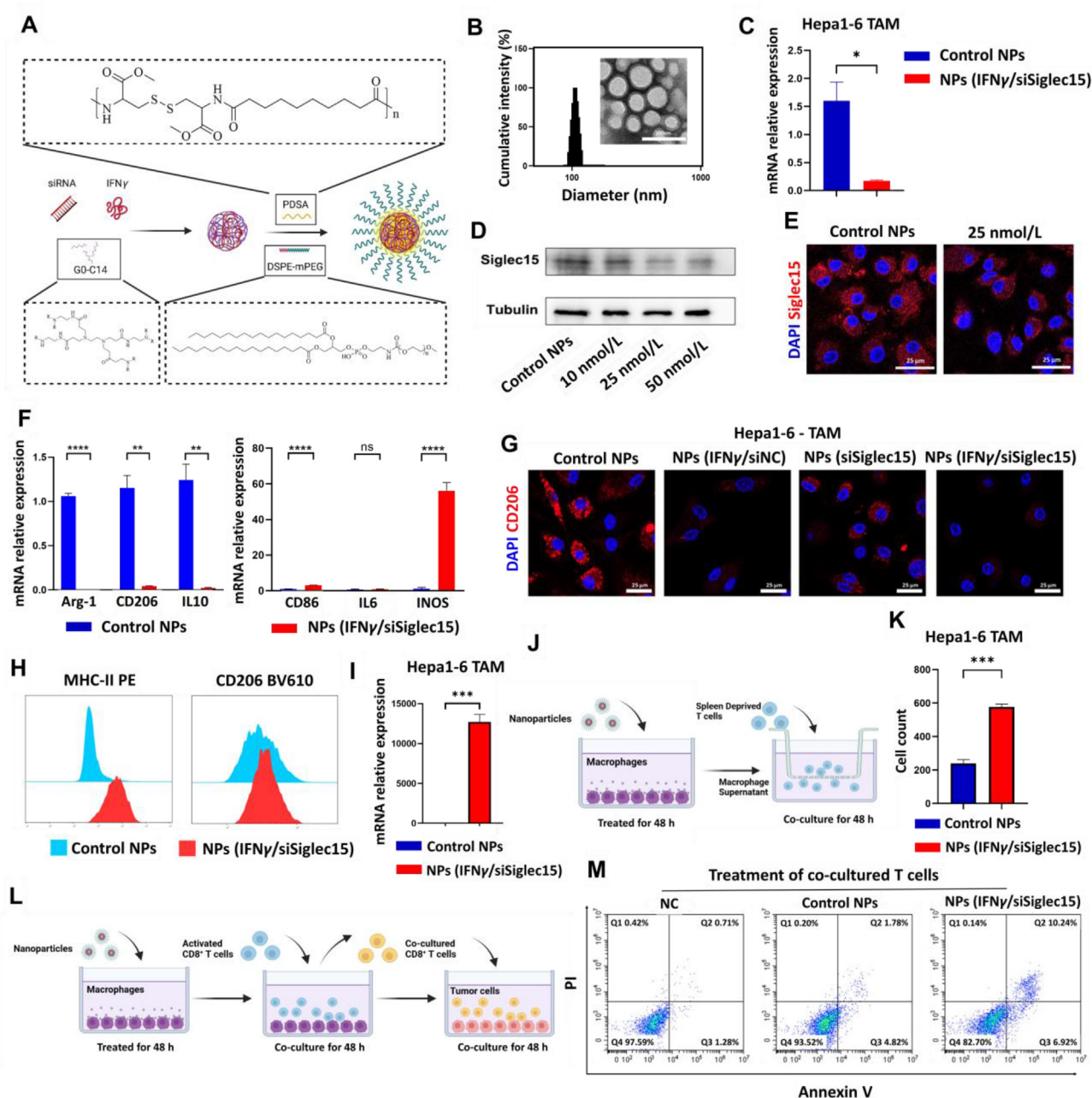


Figure 2 Characterization, gene silencing and repolarization ability of NPs (IFN γ /siSiglec15) *in vitro*. (A) Schematic illustration of reduction-responsive NPs for the delivery of siRNA and IFN γ . (B) TEM image and size distribution of NPs (IFN γ /siSiglec15) in aqueous solution. Scale bar = 200 nm. (C–E) Siglec15 expression determined by qPCR (C), western blot (D) and confocal microscopy (E), data were presented as mean \pm SEM ($n = 3$). * $P < 0.05$ vs. indicated. Scale bar = 25 μ m. (F) The expression of classic markers of M2-like macrophage (CD206, Arg-1 and IL10) and M1-like macrophage (CD86, IL6, and INOS) determined by qRT-PCR analysis of TAMs treated with NPs (IFN γ /siSiglec15). Data were presented as mean \pm SEM ($n = 3$). ns, not significant; ** $P < 0.005$, **** $P < 0.0001$ vs. indicated. (G) IF analysis of CD206 of TAMs treated with NPs (IFN γ /siSiglec15) determined by confocal microscopy. Scale bar = 25 μ m. (H) The expression of MHC-II and CD206 of TAMs treated with NPs (IFN γ /siSiglec15) determined by flow cytometric analysis. (I) CXCL9 mRNA expression of TAMs treated with NPs (IFN γ /siSiglec15). Data were presented as mean \pm SEM ($n = 3$). *** $P < 0.001$ vs. indicated (J) Schematic illustration of T cell recruiting co-culture assay of tumor-associated macrophages (TAMs), before co-culture with spleen deprived T cells, the TAMs were treated with control NPs or NPs (IFN γ /siSiglec15) for 48 h. (K) CD8 $^+$ T cells recruited by TAMs treated with NPs (IFN γ /siSiglec15) determined by flow cytometric analysis. Data were presented as mean \pm SEM ($n = 3$). *** $P < 0.001$ vs. indicated. (L) Schematic illustration of T cell recruiting co-culture assay of tumor-associated macrophages (TAMs), before co-cultured with spleen deprived T cells, the TAMs were treated with control NPs or NPs (IFN γ /siSiglec15) for 48 h. (M) Flow cytometric detection of Hepa1-6 cell apoptosis after co-culture with CD8 $^+$ T cells. The schematic illustration in this figure was created using BioRender (<https://biorender.com>).

encapsulation efficiency of siSiglec15 and IFN γ was determined as $\sim 70\%$ and $\sim 60\%$, respectively. A high concentration of GSH (10 mmol/L) could induce the rapid release of Cy5 labeled-siRNA, showing a good reduction response (Supporting Information Fig. S5A). We used confocal laser scanning microscopy (CLSM) to investigate the intracellular trafficking of NPs (IFN γ /siSiglec15) in BMDMs (Fig. S5B). When the cells were exposed to the NPs (IFN γ /siSiglec15) for 0.5 h, Cy3 labeled IFN γ and Cy5 labeled siRNA were mostly found in endo/lysosomes, indicating that the NPs (IFN γ /siSiglec15) were taken up through endocytosis. Two hours after treatment, a decrease in the co-localized Cy3 labeled IFN γ and Cy5 labeled siRNA and endo/lysosome signals suggested that the NPs (IFN γ /siSiglec15) had escaped from the endo/lysosomes (Fig. S5B).

After the preparation of NPs (IFN γ /siSiglec15), we investigated the Siglec15 knockdown efficiency of NPs. NPs reduced the mRNA expression level of Siglec15 significantly (Fig. 2C). NPs (25 nmol/L as the minimum concentration) could effectually silence the protein expression of Siglec15 confirmed by the western blot (Fig. 2D, Supporting Information Fig. S6). Similarly, the protein expression of Siglec15 (red fluorescence intensity) on TAMs was also reduced by NPs (25 nmol/L) on a confocal fluorescence microscope (Fig. 2E).

IFN γ is reported to promote the M1 phenotype in macrophages. We examined the repolarization effect of NPs (IFN γ /siSiglec15) on TAMs. For the TAMs treated by NPs, the mRNA expression of Arg-1, CD206, and IL-10 (makers of M2) was decreased and that of CD86, IL6, and iNOS (makers of M1) were up-regulated significantly (Fig. 2F). Compared to the control group, NPs (siSiglec15) could reduce the expression of CD206 (red fluorescence) on a confocal fluorescence microscope. Moreover, NPs (IFN γ /siNC) and NPs (IFN γ /siSiglec15) could significantly reduce the CD206 expression level compared to NPs (siSiglec15) (Fig. 2G). In addition, the protein expression of MHC-II (surface maker of M1) was up-regulated and CD206 (surface maker of M2) was down-regulated significantly in flow cytology analysis (Fig. 2H).

Previous studies have pointed out that pro-inflammatory chemokines including CCL5, CXCL10, and CXCL9 could recruit T cell infiltration⁵. We have found that after being treated with IFN γ , macrophages produced high levels of these chemokines, especially CXCL9 (Fig. S3D). The NPs (IFN γ /siSiglec15) also enhanced the production of CXCL9 in TAMs, which was detected by qPCR (Fig. 2I). We also conducted T cell chemotaxis experiment *in vitro* to investigate the T cell chemotaxis ability of the chemokines secreted by TAMs. We have found the TAMs treated with NPs (in the bottom chamber) could efficiently recruit CD8⁺ T cells (in the top chamber) (Fig. 2J and K).

We conducted T cell killing experiments using a co-culture assay of TAMs or tumor cells with CD8⁺ T cells (Fig. 2L). Initially, T cells were co-cultured with NPs (IFN γ +siSiglec15) transfected macrophages for 48 h. Subsequently, activated T cells were co-cultured with tumor cells directly to investigate the immune cell-mediated killing effect. Our findings revealed an increase in tumor cell apoptosis in the NPs (IFN γ +siSiglec15) group, indicating that siRNA delivery by NPs (IFN γ +siSiglec15) could enhance CD8⁺ T cell anti-tumor immunity *via* Siglec15 gene silencing in macrophages (Fig. 2M).

3.4. *In vivo* gene silencing and macrophage repolarization

Next, we assessed the ability of the NPs (IFN γ /siSiglec15) to repolarize macrophages to M1 and CD8⁺ T cell infiltration levels *in vivo*. Pharmacokinetics and biodistribution of NPs (IFN γ /

siSiglec15) were first investigated. As shown in Fig. 3A, encapsulating siRNA into nanoparticles could prolong siRNA's blood circulation time significantly in contrast to naked siRNA which was rapidly cleared from the blood. This is mainly attributed to the PEG outer layer of the nanoparticles, which helps them evade phagocytosis by macrophages, resulting in a prolonged circulation time in the bloodstream. Biodistribution assays were performed by injection of free Cy5-siRNA or Cy5-siRNA loaded NPs, mice with tumors were harvested after 24 h, and the Cy5-siRNA loaded NPs showed much higher tumor accumulation compared to free cy5-siRNA ($n = 3$) (Fig. 3B). After collecting the organ supernatant of the tumor, the fluorescence signal of Cy5-siRNA loaded NPs was more 3 times higher than that of free siRNA (Fig. 3C). The nanoparticles were found to accumulate in the kidney but not in the liver. Factors such as small size, negative charge, high water solubility, high density, and intravenous drug delivery all contributed to the targeted accumulation of nanoparticles in the kidney^{31,32}, which was consistent with our previous studies²¹. Taken together, these results indicated the favorable tumor-targeting ability of NPs (IFN γ /siSiglec15) *in vivo*.

We next applied intravenously injection of the NPs (IFN γ /siSiglec15) into the subcutaneous mice model to investigate their *in vivo* repolarizing efficacy and T cells infiltration level (Fig. 3D). We first examined Siglec15 expression by Western blot and immunohistochemistry (IHC) analysis of tumor tissues treated with the Control NPs, NPs (siSiglec15), NPs (IFN γ /siNC) and NPs (IFN γ /siSiglec15), the NPs could concurrently down-regulate the expression of Siglec15 (Fig. 3E and F). We exhibited the macrophage cell and T cell sorting step in the flow cytometry (Supporting Information Fig. S7). Gating on cell size and intracellular granularity, and then dead cells were excluded by fixable viability dye (FVD) staining on the APC-A750 channel before the surface stain. Live cells were next divided into macrophages (CD11b⁺) and T cells (CD3⁺) and finally, the surface stain of CD206, MHC-II, CD4, and CD8 respectively to analyze the proportion of macrophages of the M1 and M2 types, as well as CD4⁺ T cell and CD8⁺ T cell, in the tumor tissues respectively. The phenotype of intra-tumoral TAMs can be repolarized from tumor-promoting M2-like to tumor-suppressing M1-like, as demonstrated by decreased CD206⁺/F480⁺ cells and increased MHC-II⁺/F480⁺ cells in the flow cytometry (Fig. 3G and H, Supporting Information Fig. S8). Meanwhile, the protein expression of CD206 (red fluorescence) in the intra-tumoral tissue sections was significantly reduced (Fig. 3J). As Fig. 3I and Supporting Information Fig. S9 shown, NPs (IFN γ /siSiglec15) had increased intra-tumoral T cell infiltration compared with NPs (IFN γ /siNC) and NPs (Siglec15). When NPs (IFN γ /siSiglec15) were combined with anti-PD1, the level of infiltration of CD8⁺ T cells was more significantly increased compared to anti-PD1 alone. Meanwhile, CD8 expression in the intra-tumoral tissue sections was significantly increased after being treated by NPs (IFN γ /siSiglec15) (Fig. 3K).

3.5. *Inhibition of tumor growth*

Based on the ability of NPs (IFN γ /siSiglec15) for M1 phenotype polarization and T cell recruitment demonstrated above *in vitro* and *in vivo*, we next examined the antitumor ability of NPs (IFN γ /siSiglec15) for inhibiting growth of HCC in subcutaneous tumor-bearing mice. First, Hepa1-6 subcutaneous tumor-bearing C57 mouse models were established and then administered PBS, Control NPs, NPs (IFN γ /siNC), NPs (siSiglec15), NPs

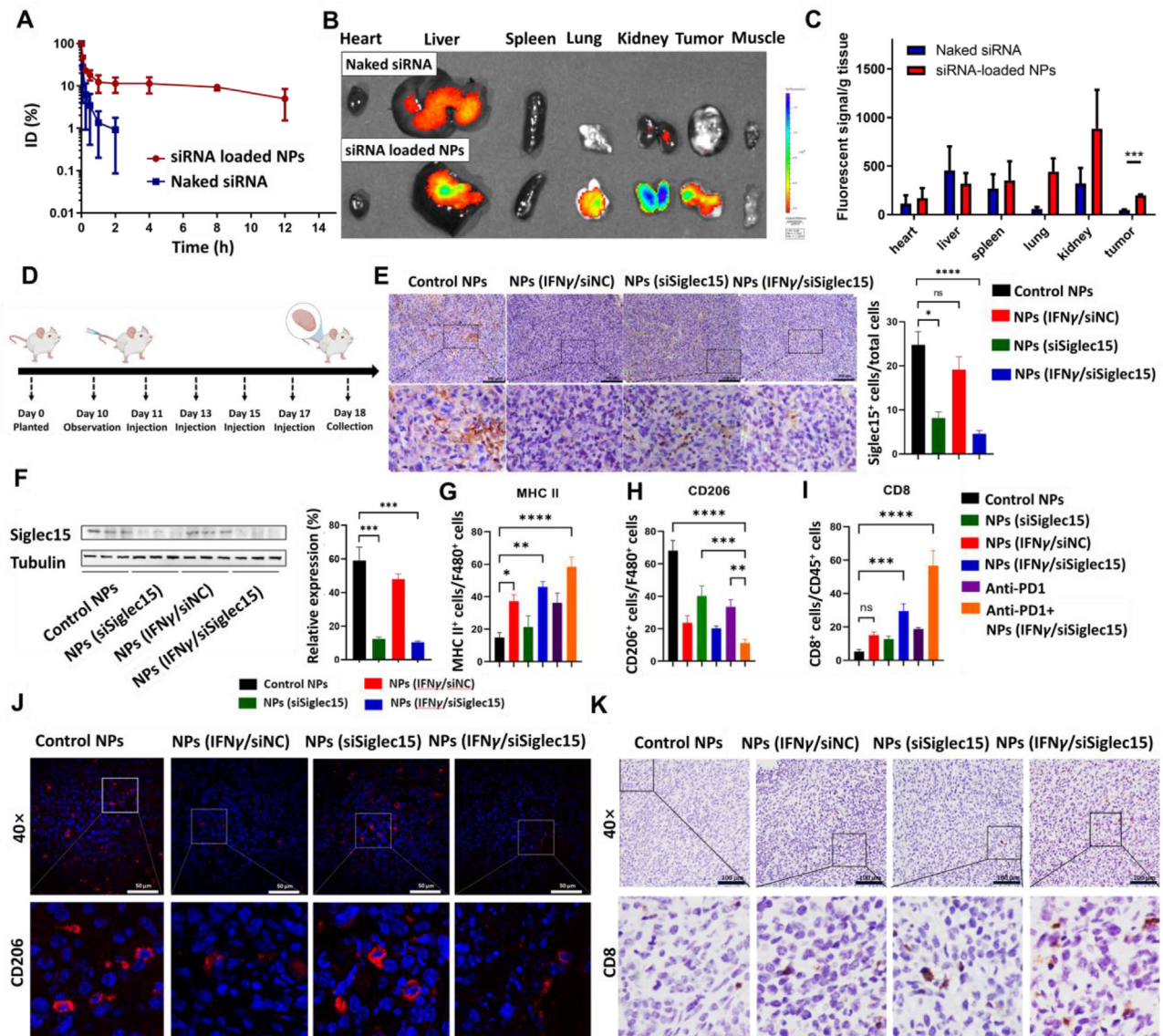


Figure 3 Blood circulation, biodistribution, gene silencing and repolarization ability of NPs (IFN γ /siSiglec15) *in vivo*. (A) Blood circulation profile of naked Cy5-siRNA and Cy5-siRNA-loaded NPs. Data were presented as mean \pm SEM ($n = 3$) (B) Overlaid fluorescence image of tumors and main organs from Hepa1-6 xenograft tumor-bearing mice at 24 h post injection of naked Cy5-siRNA and Cy5-siRNA-loaded NPs. (C) Biodistribution of naked Cy5-siRNA and Cy5-siRNA-loaded NPs quantified from (B). Data were presented as mean \pm SEM ($n = 3$), *** $P < 0.001$ vs. indicated. (D) Schematic illustration images of Hepa1-6 subcutaneous tumor-bearing mice treated with Control NPs, NPs (IFN γ /siNC), NPs (siSiglec15) and NPs (IFN γ /siSiglec15). (E, F) Siglec15 expression of Hepa1-6 xenograft tumor-bearing mice treated with Control NPs, NPs (IFN γ /siNC), NPs (siSiglec15) and NPs (IFN γ /siSiglec15) determined by IHC (Immunohistochemistry) (E) and western blot (F). Data were presented as mean \pm SEM ($n = 5$). ns, not significant; * $P < 0.05$, **** $P < 0.0001$ vs. indicated. Scale bar = 100 μ m. (G–I) Flow cytometric analysis of MHC-II $^+$ macrophages (G), CD206 $^+$ macrophages (H), and CD8 $^+$ T cells (I) of Hepa1-6 subcutaneous tumor-bearing mice treated with Control NPs, NPs (IFN γ /siNC), NPs (siSiglec15) and NPs (IFN γ /siSiglec15). Data were presented as mean \pm SEM ($n = 5$). ns, not significant; * $P < 0.05$, ** $P < 0.005$, *** $P < 0.001$, **** $P < 0.0001$ vs. indicated. (J) IF analysis of CD206 of Hepa1-6 subcutaneous tumor-bearing mice treated with Control NPs, NPs (IFN γ /siNC), NPs (siSiglec15) and NPs (IFN γ /siSiglec15). Scale bar = 50 μ m. (K) IHC analysis of CD8 $^+$ T cells of Hepa1-6 subcutaneous tumor-bearing mice treated with Control NPs, NPs (IFN γ /siNC), NPs (siSiglec15) and NPs (IFN γ /siSiglec15). Scale bar = 100 μ m.

(IFN γ /siSiglec15), anti-PD1, anti-PD1 + NPs (IFN γ /siSiglec15) every 2 days, anti-PD1 was injected every 3 days. The dose of siRNA was fixed at 0.5 nmol/mouse, and the dose of IFN γ was fixed at 5 μ g per mouse. In regard to the xenograft tumor model with an initial tumor volume of ~ 75 mm 3 , NPs (IFN γ /siSiglec15) significantly inhibited the tumor growth (Fig. 4A–C, Supporting Information Fig. S10), when combined with anti-PD1, the tumor

size was significantly reduced and 1 of the tumors disappeared within the evaluation period. In comparison to other groups, according to Ki67 and TUNEL staining of tumor cells, NPs (IFN γ /siSiglec15) were the most effective at inhibiting cell proliferation and inducing cell apoptosis (Fig. 4I).

We established an orthotopic tumor model to further investigate the combinational effect against cancer of NPs (IFN γ /siSiglec15)

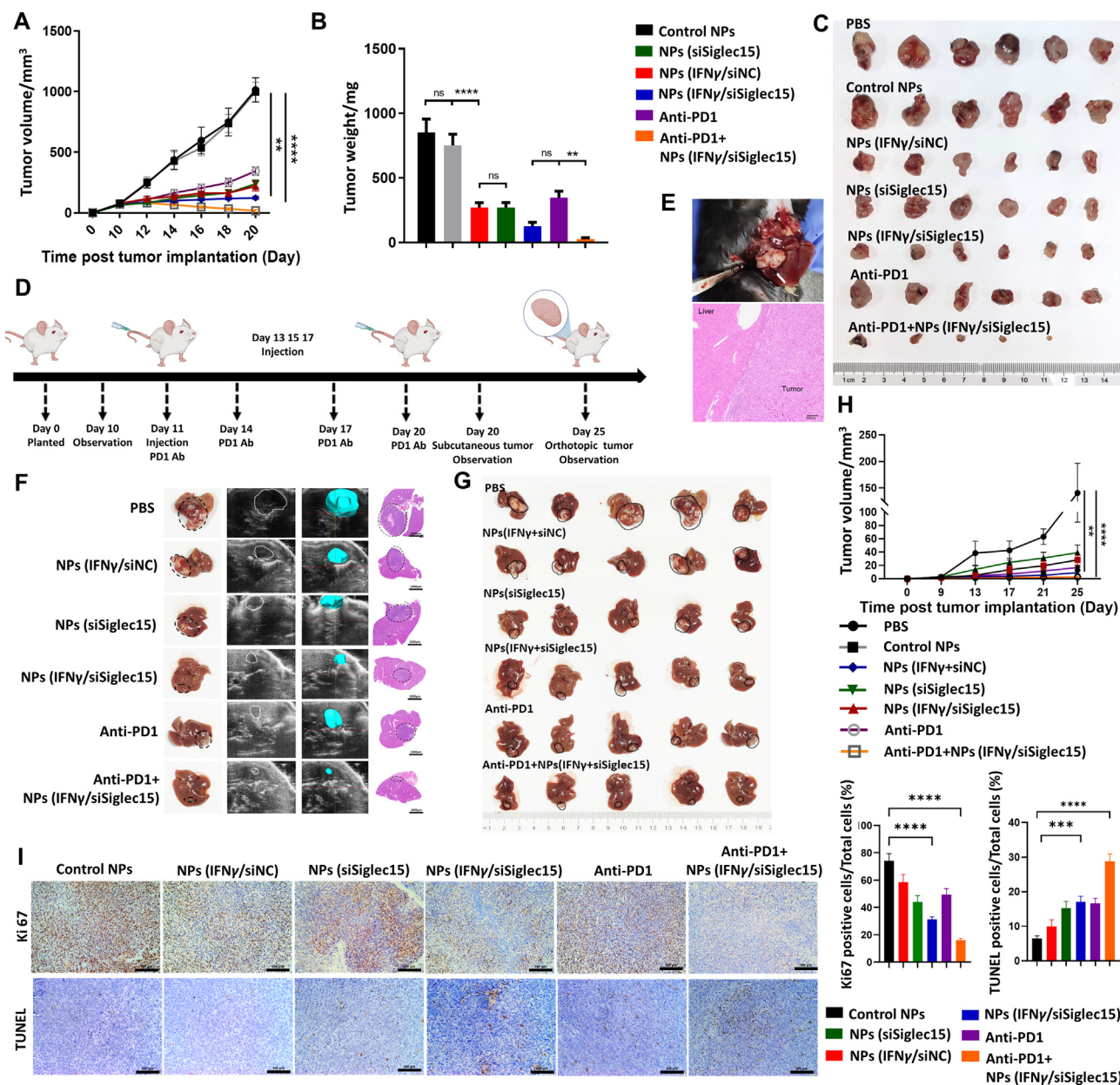


Figure 4 Antitumor efficacy of NPs (IFN γ /siSiglec15) *in vivo*. (A, B) Tumor size (A) and weight (B) of Hepa1-6 subcutaneous tumor-bearing mice. Data were presented as mean \pm SEM ($n = 6$). $**P < 0.005$, $****P < 0.0001$ vs. indicated. (C) Photograph of collected Hepa1-6 subcutaneous tumors in each group at the end point (Day 20). (D) Schematic illustration images of Hepa1-6 subcutaneous and orthotopic tumor-bearing mice treated with Control NPs, NPs (IFN γ /siINC), NPs (siSiglec15), NPs (IFN γ /siSiglec15) and anti-PD1. (E) Photograph of one representative Hepa1-6 orthotopic tumor-bearing mouse and histological section of its orthotopic tumor. The orthotopic tumor is indicated by the arrows. Scale bar = 200 μ m. (F) Representative ultrasound and H&E images of Hepa1-6 orthotopic tumor-bearing mice at the end point (Day 25). Scale bar = 1000 μ m. (G) Photograph of collected Hepa1-6 orthotopic tumors in each group at the end point (Day 25). (H) Tumor size of Hepa1-6 orthotopic tumor-bearing mice. Data were presented as mean \pm SEM ($n = 5$). $**P < 0.005$; $****P < 0.0001$ vs. indicated. (I) Ki67 and TUNEL staining of tumor tissues after systemic treatment in each group. Data were presented as mean \pm SEM ($n = 5$). $**P < 0.001$; $****P < 0.0001$ vs. indicated. Scale bar = 100 μ m.

(Fig. 4D and E). The orthotopic tumors were scanned by a small animal ultrasound machine (Vevo 2100), and 3D reconstruction was performed to monitor the tumor growth stereoscopically (Fig. 4F). As shown in Fig. 4F and G, and Supporting Information Fig. S11, NPs (IFN γ /siSiglec15) showed the strongest efficacy against tumor compared to mice treated with NPs (IFN γ /siINC) or NPs (siSiglec15). Tumors increased by approximately 10 mm³ in mice treated with NPs

(IFN γ /siSiglec15) over the 25-day evaluation period (Fig. 4G). In contrast, mice treated with NPs (IFN γ /siINC) or NPs (siSiglec15) had more than a 2-fold increase in tumor size compared to NPs (IFN γ /siSiglec15). In addition, the tumor volume of mice increased by 20 mm³ approximately when treated with anti-PD1 alone, and the mice treated with anti-PD1 + NPs (IFN γ /siSiglec15) had almost no tumor growth. All these results showed that the NPs (IFN γ /

siSiglec15) could significantly promote the polarization of macrophages to the M1 type and increase the infiltration of T cells, and improve the protective immune response, thus showing strong anti-tumor ability.

In both subcutaneous and orthotopic models, the NPs (IFN γ /siSiglec15) did not affect the mouse body weight (Supporting Information Fig. S12). NPs loaded with siRNA and IFN γ were injected intravenously into healthy mice to further evaluate potential side effects (0.5 nmol siRNA dose and 5 μ g IFN γ per mouse, $n = 3$). Following three daily injections, none of the hematological parameters showed a significant increase, including aspartate aminotransferase (AST), alanine aminotransferase (ALT), alkaline phosphatase (ALP), urea, creatinine, and total protein (TP) (Supporting Information Fig. S13). Heart, liver, spleen, lung, and kidney tissues also show no significant changes on histological examination (Supporting Information Fig. S14). We also observed that the NPs (IFN γ /siSiglec15) exhibit good stability in PBS with 10% fetal bovine serum (FBS). Our experiments showed that the size of NPs (IFN γ /siSiglec15) remained unchanged even after being incubated in serum for 24 h. We further investigated the hemolysis reaction caused by NPs (IFN γ /siSiglec15), our research findings indicated that our nanomaterials did not cause any damage to blood cell membranes (Supporting Information Fig. S15).

All these results suggested that the NPs (IFN γ /siSiglec15) showed low toxicity and good biocompatibility *in vivo*, were resistant to aggregation, and could maintain their integrity in biological fluids in this work.

4. Conclusions

We have developed a reduction-responsive nanoplatform to deliver IFN γ and siSiglec15 systemically to increase T cell infiltration and proliferation for enhanced cancer immunotherapy. The nanoplatform shows high tumor accumulation and long blood circulation. After internalization by TAMs, the loaded IFN γ and siSiglec15 could be rapidly released to respectively repolarize TAMs phenotype and silence Siglec15 expression. With this TAMs repolarization to enhance CXCL9 secretion for T cell infiltration and Siglec15 silencing to increase T cell proliferation, the tumor growth is significantly suppressed when combining the anti-PD1 with the NPs loading IFN γ and siSiglec15. The strategy developed in this work could be used as a promising therapeutic modality for enhanced cancer immunotherapy.

Acknowledgments

This work was supported by the National Natural Science Foundation of China (82171944, 81873899, China), the Natural Science Foundation of Guangdong Province (2021A1515012611, China), the National Natural Science Foundation of China (82171952, 81801719, China), Postdoctoral Research and Development Fund Project of West China Hospital (2023HXBH063, China). The authors acknowledged the Sun Yat-sen Memorial Hospital of Sun Yat-sen University and West China Hospital of Sichuan University for technical assistance.

Author contributions

Xiaodi Liu and Xiaoding Xu wrote the manuscript. Xiaodi Liu, Qi Zhang, and Xiaolin Xu prepared Figs. 1 and 2, Xiaodi Liu, Yixia

Liang and Yanni Xu prepared Fig. 3, Xiaodi Liu, Yan Cai and Shiyu Xiong prepared Fig. 4. Jincheng Cao, Ye Wu and Qiang Lu prepared the Scheme. Xiaodi Liu, Qi Zhang and Baoming Luo prepared the supporting information. All authors read and approved the final manuscript.

Conflicts of interest

The authors declare no conflicts of interest.

Appendix A. Supporting information

Supporting data to this article can be found online at <https://doi.org/10.1016/j.apsb.2023.07.012>.

References

- Hinshaw DC, Shevde LA. The tumor microenvironment innately modulates cancer progression. *Cancer Res* 2019;**79**:4557–66.
- Fu T, Dai LJ, Wu SY, Xiao Y, Ma D, Jiang YZ, et al. Spatial architecture of the immune microenvironment orchestrates tumor immunity and therapeutic response. *J Hematol Oncol* 2021;**14**:98.
- Reina-Campos M, Scharping NE, Goldrath AW. CD8⁺ T cell metabolism in infection and cancer. *Nat Rev Immunol* 2021;**21**:718–38.
- House IG, Savas P, Lai J, Chen A, Oliver AJ, Teo ZL, et al. Macrophage-derived CXCL9 and CXCL10 are required for antitumor immune responses following immune checkpoint blockade. *Clin Cancer Res* 2020;**26**:487–504.
- Pascual-García M, Bonfill-Teixidor E, Planas-Rigol E, Rubio-Perez C, Iurlaro R, Arias A, et al. LIF regulates CXCL9 in tumor-associated macrophages and prevents CD8⁺ T cell tumor-infiltration impairing anti-PD1 therapy. *Nat Commun* 2019;**10**:2416.
- Dangaj D, Bruand M, Grimm AJ, Ronet C, Barras D, Duttagupta PA, et al. Cooperation between constitutive and inducible chemokines enables T cell engraftment and immune attack in solid tumors. *Cancer Cell* 2019;**35**:885–900.
- Tokunaga R, Zhang W, Naseem M, Puccini A, Berger MD, Soni S, et al. CXCL9, CXCL10, CXCL11/CXCR3 axis for immune activation—a target for novel cancer therapy. *Cancer Treat Rev* 2018;**63**:40–7.
- Bedognetti D, Spivey TL, Zhao Y, Uccellini L, Tomei S, Dudley ME, et al. CXCR3/CCR5 pathways in metastatic melanoma patients treated with adoptive therapy and interleukin-2. *Br J Cancer* 2013;**109**:2412–23.
- Wu J, Xiao X, Jia H, Chen J, Zhu Y, Zhao P, et al. Dynamic distribution and expression *in vivo* of the human interferon gamma gene delivered by adenoviral vector. *BMC Cancer* 2009;**9**:55.
- Sun J, Lu Q, Sanmamed MF, Wang J. Siglec-15 as an emerging target for next-generation cancer immunotherapy. *Clin Cancer Res* 2021;**27**:680–8.
- Hu J, Yu A, Othmane B, Qiu D, Li H, Li C, et al. Siglec15 shapes a non-inflamed tumor microenvironment and predicts the molecular subtype in bladder cancer. *Theranostics* 2021;**11**:3089–108.
- Wang J, Sun J, Liu LN, Flies DB, Nie X, Toki M, et al. Siglec-15 as an immune suppressor and potential target for normalization cancer immunotherapy. *Nat Med* 2019;**25**:656–66.
- Li TJ, Jin KZ, Li H, Ye LY, Li PC, Jiang B, et al. SIGLEC15 amplifies immunosuppressive properties of tumor-associated macrophages in pancreatic cancer. *Cancer Lett* 2022;**530**:142–55.
- Ji G, Ma L, Yao H, Ma S, Si X, Wang Y, et al. Precise delivery of obeticholic acid *via* nanoapproach for triggering natural killer T cell-mediated liver cancer immunotherapy. *Acta Pharm Sin B* 2020;**10**:2171–82.
- Xu Y, Xiong J, Sun X, Gao H. Targeted nanomedicines remodeling immunosuppressive tumor microenvironment for enhanced cancer immunotherapy. *Acta Pharm Sin B* 2022;**12**:4327–47.

16. Mccaffrey AP, Meuse L, Pham TT, Conklin DS, Hannon GJ, Kay MA. RNA interference in adult mice. *Nature* 2002;**418**:38–9.
17. Whitehead KA, Langer R, Anderson DG. Knocking down barriers: advances in siRNA delivery. *Nat Rev Drug Discov* 2009;**8**:129–38.
18. Shi J, Kantoff PW, Wooster R, Farokhzad OC. Cancer nanomedicine: progress, challenges and opportunities. *Nat Rev Cancer* 2017;**17**:20–37.
19. Tseng YC, Mozumdar S, Huang L. Lipid-based systemic delivery of siRNA. *Adv Drug Deliv Rev* 2009;**61**:721–31.
20. Hanahan D, Weinberg RA. Hallmarks of cancer: the next generation. *Cell* 2011;**144**:646–74.
21. Xu X, Wu J, Liu Y, Saw PE, Tao W, Yu M, et al. Multifunctional envelope-type siRNA delivery nanoparticle platform for prostate cancer therapy. *ACS Nano* 2017;**11**:2618–27.
22. Liu Y, Xu CF, Iqbal S, Yang XZ, Wang J. Responsive nanocarriers as an emerging platform for cascaded delivery of nucleic acids to cancer. *Adv Drug Deliv Rev* 2017;**115**:98–114.
23. Saw PE, Yao H, Lin C, Tao W, Farokhzad OC, Xu X. Stimuli-responsive polymer-prodrug hybrid nanoplatform for multistage siRNA delivery and combination cancer therapy. *Nano Lett* 2019;**19**:5967–74.
24. Cao S, Saw PE, Shen Q, Li R, Liu Y, Xu X. Reduction-responsive RNAi nanoplatform to reprogram tumor lipid metabolism and repolarize macrophage for combination pancreatic cancer therapy. *Bio-materials* 2022;**280**:121264.
25. Ma L, Hernandez MO, Zhao Y, Mehta M, Tran B, Kelly M, et al. Tumor cell biodiversity drives microenvironmental reprogramming in liver cancer. *Cancer Cell* 2019;**36**:418–30.
26. Xu X, Wu J, Liu S, Saw PE, Tao W, Li Y, et al. Redox-responsive nanoparticle-mediated systemic rnaï for effective cancer therapy. *Small* 2018;**14**:e1802565.
27. Rodriguez-García A, Lynn RC, Poussin M, Eiva MA, Shaw LC, O'Connor RS, et al. Car-t cell-mediated depletion of immunosuppressive tumor-associated macrophages promotes endogenous anti-tumor immunity and augments adoptive immunotherapy. *Nat Commun* 2021;**12**:877.
28. Bai R, Yuan C, Sun W, Zhang J, Luo Y, Gao Y, et al. Nek2 plays an active role in tumorigenesis and tumor microenvironment in non-small cell lung cancer. *Int J Biol Sci* 2021;**17**:1995–2008.
29. Cao X, Zhou Y, Mao F, Lin Y, Zhou X, Sun Q. Identification and characterization of three Siglec15-related immune and prognostic subtypes of breast-invasive cancer. *Int Immunopharm* 2022;**106**:108561.
30. Li B, Zhang B, Wang X, Zeng Z, Huang Z, Zhang L, et al. Expression signature, prognosis value, and immune characteristics of Siglec-15 identified by pan-cancer analysis. *OncImmunology* 2020;**9**:1807291.
31. Wang G, Li Q, Chen D, Wu B, Wu Y, Tong W, et al. Kidney-targeted rhein-loaded liponanoparticles for diabetic nephropathy therapy via size control and enhancement of renal cellular uptake. *Theranostics* 2019;**9**:6191–208.
32. Huang Y, Wang J, Jiang K, Chung EJ. Improving kidney targeting: the influence of nanoparticle physicochemical properties on kidney interactions. *J Control Release* 2021;**334**:127–37.